Scientific Research Publishing

Atmospheric and Climate Sciences, 2025, 15(2), 373-390
https://www.scirp.org/journal/acs
ISSN Online: 2160-0422
ISSN Print: 2160-0414

Analysis of Geomagnetic Storm Effects on Ionospheric Vertical Drifts over the East African Low Latitude Region

Duncan Niwamanya[1,2], Valence Habyarimana[2], Edward Jurua[2]

[1]Department of Physics, Kabale University, Kabale, Uganda
[2]Department of Physics, Mbarara University of Science and Technology, Mbarara, Uganda
Email: dunconiwax@gmail.com

How to cite this paper: Niwamanya, D., Habyarimana, V. and Jurua, E. (2025) Analysis of Geomagnetic Storm Effects on Ionospheric Vertical Drifts over the East African Low Latitude Region. *Atmospheric and Climate Sciences*, **15**, 373-390.
https://doi.org/10.4236/acs.2025.152019

Received: January 28, 2025
Accepted: March 25, 2025
Published: March 28, 2025

Abstract

The geomagnetic storm effect on ionospheric vertical $\mathbf{E} \times \mathbf{B}$ drift is analysed using Communication/Navigation Outage and Forecasting System (C/NOFS) Satellite data, magnetometer data, and solar wind data, over the East African low latitude region during the period 2008-2015. We identified a total of 608 corotating interaction region (CIR)-driven and 23 coronal mass ejection (CME)-driven geomagnetic storms in this study. Most of the CIR-driven storms were observed during the declining phase of solar cycle 24 in 2015. The CME-driven storms, on the other hand, were dominant during the near maximum phase of the solar cycle 24 in 2012. The C/NOFS satellite data was found to be consistent with magnetometer observations in identifying both upward and downward vertical $\mathbf{E} \times \mathbf{B}$ drift occurrence. The common result of analysed CME-driven geomagnetic storms was enhancement in $\mathbf{E} \times \mathbf{B}$ drifts due to presence of eastward prompt penetrating electric fields (PPEFs) during the storm main phase. There was also a decrease in $\mathbf{E} \times \mathbf{B}$ due to the decrease in horizontal component of the magnetic field (ΔH) during the recovery phases of the CME-driven storms. This is a manifestation of downward $\mathbf{E} \times \mathbf{B}$ drifts associated with westward electric field, which is due to the disturbance dynamo contribution. During CIR-driven geomagnetic storms, the storm's main phases were also dominated by downward $\mathbf{E} \times \mathbf{B}$ drifts associated with westward electric field, which is due to disturbance dynamo.

Keywords

Prompt Penetration Electric Fields, Disturbed Dynamo Electric Fields, Geomagnetic Storms, Vertical $\mathbf{E} \times \mathbf{B}$ Drifts

1. Introduction

The low latitude ionosphere is significantly disturbed rendering space-based navigation unreliable during extreme space weather events such as geomagnetic storms [1]-[3]. During the onset of either Corotating Interaction Region (CIR) or Coronal Mass Ejection (CME)-driven geomagnetic storms, there is always modification of low/equatorial latitude electric fields, mainly due to equatorward neutral winds, Disturbed Dynamo Electric Fields (DDEFs) and Prompt Penetrating Electric Fields (PPEFs) of magnetospheric origin [4]. To alleviate the effect of these space weather events, considerable efforts are being made to understand and model the low/equatorial latitude electrodynamics [5]-[8]. However, over the East African low latitude, the effect that these space weather events have on the ionospheric electrodynamics is not yet well studied due to inadequate ground-based instrumentation dedicated to vertical $\mathbf{E} \times \mathbf{B}$ drifts measurement [9]. Hence, the response of the low latitude ionosphere to magnetospheric disturbances such as solar flares, CIRs and CMEs still remains one of the issues related to space weather studies. These responses become remarkable during major geomagnetic storms [10].

Geomagnetic storms are changes in the magnetosphere that are induced by the interaction of solar wind and the Earth's magnetosphere [11] [12]. The solar energetic events, such as CMEs and CIRs, are the principal causes of geomagnetic storms [13]. It is important to understand large ionospheric perturbations that are brought about by these geomagnetic storms because they can significantly disrupt satellite navigation, spacecraft, radio communications and even power grids [14]. The study of ionospheric response to CIRs and CMEs gained attention decades ago [9] [15]-[18]. With the comparison of different types of ionospheric response brought about by different disturbance sources from solar activity and interplanetary solar wind, scientists can comprehensively understand the morphological changes and physical processes of ionospheric storms. This helps them to easily predict the ionospheric disturbance state according to different solar wind conditions [17].

The rate at which CMEs and CIRs occur follows the 11-year solar cycle of sunspot activity, with CMEs occurring more frequently during solar maximum phase and CIRs occurring most during the solar minimum/declining phase of the solar cycle [15] [16]. The energy associated with the solar wind also varies over the solar cycle, with higher energy levels during solar maximum and lower levels during solar minimum, leading to distinct space weather effects throughout the cycle [19]. The CIR-driven storms are characterised by long-duration recovery phase, which may last for days to many weeks while CME-driven geomagnetic storms recovery phases can last for about 1 or 2 days [16]. During CME- and CIR-driven geomagnetic storms, there is always either a decrease or increase in the electron density in the ionosphere [13]. The response of the ionosphere to either CME or CIR-driven geomagnetic storms at different latitudes has been studied [17] [20]-[26]. [20] showed that during CIR-driven storm on 9 August 2008, a decrease in $\mathbf{E} \times \mathbf{B}$

drift from a daytime counter electrojet (CEJ) led to a significant ionospheric density reduction in the African sector. This observation is consistent with the idea that the equatorial electrojet (EEJ) and thus east-west electric field is the main governing mechanism for both E- and F-region electrodynamics. Their study was limited to CIR-driven storm, which is usually categorized as a moderate storm and it investigated only the effect of the storm on a single location. [21] studied CIR-induced magnetic storms during solar minimum and their effects on low latitude ionosphere and geomagnetic field over the Indian sector. They found that during the CIR-driven geomagnetic storms, the short lived penetration of high latitude electric fields to equatorial ionosphere exists during main phase of the geomagnetic storm as inferred from changes in EEJ.

Electric fields originating in the magnetosphere have the ability to penetrate the low-latitude and equatorial ionosphere. These penetrating electric fields result in vertical motion and they usually restructure the F-region density profiles because the recombination rate depends on the height [27]. At low latitudes, an enhanced eastward electric field will uplift the equatorial ionospheric plasma particles. This makes the equatorial F-region almost empty and at about 15˚ plasma density gets enhanced [28]. At mid latitudes, the $\mathbf{E} \times \mathbf{B}$ drift will move the ionospheric plasma upward which increases the plasma density. At high latitudes, the enhanced electric field causes storm enhanced density in the dusk sector which is subsequently transported to the polar ionosphere [2]. At the equator, the eastward current due to the vertical Hall voltage and Pedersen current due to the eastward electric field combine to enhance EEJ current in the E-region [28]. The EEJ current generates an east-west electric field in the E-region that is conveyed along the magnetic field to the F-region where they are responsible for either upward or downward $\mathbf{E} \times \mathbf{B}$ force [29]. The $\mathbf{E} \times \mathbf{B}$ force can either drive the F-region plasma to higher or lower altitudes. In the case of upward $\mathbf{E} \times \mathbf{B}$ drift, the plasma that is lifted to higher altitudes diffuses north and south along magnetic field lines to form two belts of high ionization density around magnetic dip latitudes [20]. The magnitude and direction of $\mathbf{E} \times \mathbf{B}$ drift can either be estimated from the day time EEJ observations using a pair of ground-based magnetometers [30] or Incoherent Scatter Radar (ISR) [31] or satellites [32].

Modification of equatorial/low latitude electric fields during storm conditions is mainly associated with ionospheric disturbed dynamo [33] and prompt penetrating electric fields [34]. Usually, PPEF is an eastward electric field, and therefore enhances vertical $\mathbf{E} \times \mathbf{B}$ drift during local daytime in low latitude ionosphere [34]. The effect of these penetration electric fields on vertical $\mathbf{E} \times \mathbf{B}$ drifts during both intense and moderate geomagnetic storms induced by CMEs and CIRs, respectively over the East African low latitude region is still an area of interest to supplement the already existing literature about geomagnetic storm effects. Therefore, there is a need to analyse the geomagnetic storm effects on the ionospheric vertical drifts over the East African low latitude region. Studies have been conducted with regard to the behavior of electric fields during geomagnetic storms at

different latitudes in different longitudinal sectors [2] [9] [20] [21] [27]. However, a few of them have been carried out over the African low latitude region using ground based magnetometer data [9]. This could partly be attributed to lack of multiple ground based instruments. Continuous investigation, especially over the low latitude ionosphere where variations of the ionospheric parameters have been recorded due to Equatorial Ionization Anomaly (EIA) and EEJ, is still required [9]. Using magnetometer data, Communication/Navigation Outage and Forecasting System (C/NOFS) satellite data and geomagnetic data from World Data Center for Geomagnetism, Kyoto University, the effects of CME and CIR-driven geomagnetic storms on the ionospheric vertical drifts over the East African low latitude region has been carried out in this study. Studies of ionospheric electric fields over the low latitude during geomagnetic storms are very important for understanding global ionospheric disturbances and for space weather applications [20].

2. Data and Methods

2.1. Data Sources

The disturbance storm time (Dst) and planetary k (Kp) indices were downloaded from Kyoto University website: http://wdc.kugi.kyoto-u.ac.jp/dstae/index.html and Potsdam website: http://www.gfz.de/kp-index/, respectively. The in situ vertical $\mathbf{E} \times \mathbf{B}$ drift data were estimated from the Ion Velocity Meter (IVM) measurements on board C/NOFS satellite (http://spdf.gsfc.nasa.gov/pub/data/cnofs/cindi/). Magnetometer data was obtained from African Meridian B-Field Education and Research (AMBER) magnetometers (http://magnetometers.bc.edu/) and International Real-time Magnetic Observatory Network (INTERMAGNET) that monitors the global Earth's magnetic field (http://www.intermagnet.org/). The location of magnetometer stations and C/NOFS data coverage is provided in **Figure 1**.

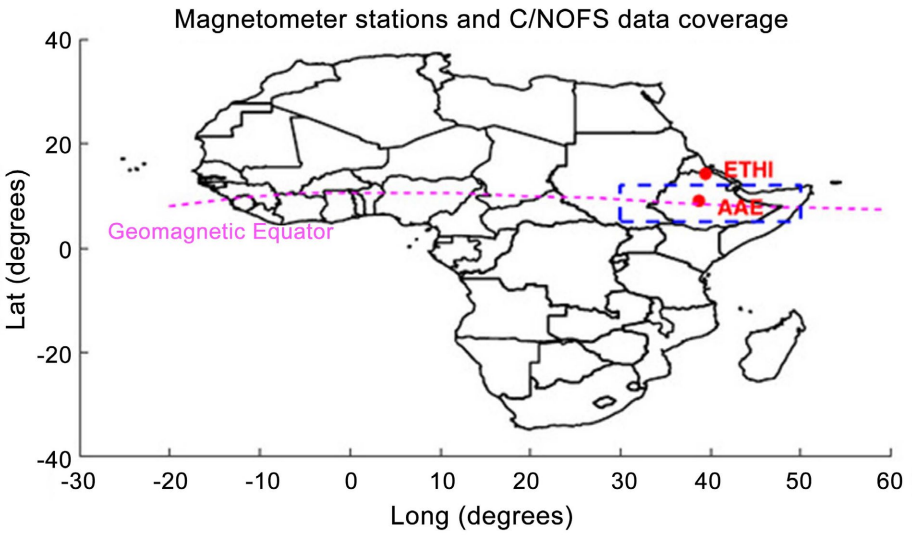

Figure 1. Location of magnetometer stations (red dots), the spatial coverage of C/NOFS data (inside the blue surface) within an altitude of 400 - 550 km [35].

2.2. Methods

To identify either a CME- or CIR-driven geomagnetic storm, the Dst and kp indices between 2008 and 2015 were used. A geomagnetic storm was considered as the one whose kp ≥ 3. The CIR-driven storms were taken to be those whose Dst index lay within the range −100 nT < Dst < −25 nT [15]. The classification is based on the minimum Dst value reached during storm occurrence. Storms within the range −100 nT < Dst < −50 nT were categorised as moderate while those within the range −50 nT < Dst < −25 nT were categorised as weak. The CME-driven storms were considered as strong and taken to be those with Dst < −100 nT [15]. To select the CME and CIR events, we also used the following existing catalogues: http://www.srl.caltech.edu/ACE/ASC/DATA/level3/icmetable2.htm and https://www.helcats-fp7.eu/catalogues/wp5_cat.html respectively. A statistical distribution of the storms during various time scales as a function of year and season was carried out. The differences in the recovery phases of CME- and CIR-driven storms were also considered. The CIR-driven storms were considered to be those with long-duration recovery phases that lasted from days to many weeks [26]. In contrast, the CME-driven storms were considered to be those with recovery phase lasting for 1 or 2 days [16].

The horizontal component of the Earth's magnetic field (H-component) data at Addis Ababa, AAE (geog. 9.03˚N, 38.7˚E, geom. 0.9˚N, 110.5˚E), and Adigrat, ETHI (geog. 14.3˚N, 39.5˚E, geom. 6.0˚N, 111.1˚E), both in Ethiopia were utilised. The H-component data sets obtained at ETHI station were subtracted from those at AAE to remove the Dst-derived ring current and the global solar quiet dynamo components of the magnetic field [36] [37]. This is because equatorial and low latitude magnetometers measure magnetic fields due to the same currents from different sources such as magnetopause, ring currents, main field, solar quiet Sq, and field aligned current (FAC), but in addition, EEJ currents are also observed at equatorial station [38]. The resulting difference provides a general perturbation of magnetic field due to the influence of EEJ, which is the basis for daytime vertical drift estimation [30] [37].

Data from the Ion Velocity Meter (IVM) instrument on board C/NOFS satellite were used to extract vertical $\mathbf{E} \times \mathbf{B}$ drifts. The IVM instrument consists of two different sensors, a retarding potential analyzer (RPA) and an ion drift meter (IDM). The RPA is responsible for measuring ion temperature, ion composition, and the component of the ion velocity in the ram (satellite velocity) direction (Vx). The two orthogonal components of the ion drift velocity (Vy and Vz), perpendicular to the satellite ram direction, are measured by an IDM [38]. The Vz component, near the magnetic equator, is normally considered as an estimator of vertical plasma drifts [38]. To limit the impact of altitude variations, measurements restricted to altitudes range of 400 - 550 km [37] [39] [40] during 2008-2015 were considered. This is because the accuracy of IVM depends on the O^+ concentration [29] [37] [41]. The C/NOFS ion drift observations used were within ±60 m/s, considering possible geomagnetic disturbances. In an effort to minimize potential

outliers associated with C/NOFS vertical ion plasma drift data, the median and scaled median absolute deviation were employed [42] during the entire period of analysis. This filtering method has been previously used in related analyses [29] [43] [44]. This was done to remove abnormally large deviations of the data from the mean diurnal vertical pattern. Drift meter high quality data flags were first applied to the C/NOFS satellite data to ensure that only good data is used [29]. After removing outliers, the C/NOFS data were averaged in 5-min intervals for each day and considered as vertical $\mathbf{E} \times \mathbf{B}$ drift observations.

To analyse the geomagnetic storm effects on ionospheric vertical drifts, the archived $\mathbf{E} \times \mathbf{B}$ drift data from magnetometers were used. The geomagnetic storm effects on ionospheric vertical drifts were identified by calculating the perturbation in $\mathbf{E} \times \mathbf{B}$ values using Equation (1):

$$\left(\mathbf{E}\times\mathbf{B}\right)_{\text{perturbation}} = \frac{\left(\mathbf{E}\times\mathbf{B}\right)-\left(\mathbf{E}\times\mathbf{B}\right)_{\text{m}}}{\left(\mathbf{E}\times\mathbf{B}\right)_{\text{m}}}\times 100\%, \tag{1}$$

where $(\mathbf{E} \times \mathbf{B})_{\text{m}}$ is the monthly median of $\mathbf{E} \times \mathbf{B}$. The $\mathbf{E} \times \mathbf{B}$ perturbations were computed when there were either CME-driven or CIR-driven storms. The $\mathbf{E} \times \mathbf{B}$ perturbations were plotted against Dst index and the variations in $\mathbf{E} \times \mathbf{B}$ were observed. The EEJ variations imply the electric field changes at equatorial station which also alters the equatorial $\mathbf{E} \times \mathbf{B}$ drifts [21].

3. Results and Discussion

Table 1 shows the number of CIR- and CME-driven geomagnetic storms considered during the period 2008 to 2015. A total of 608 CIR-driven and 23 CME-driven geomagnetic storms were considered.

Table 1. Number of CIR- and CME-driven geomagnetic storms identified during the period 2008 to 2015.

Year	CIR-driven storms	CME-driven storms
2008	57	0
2009	16	0
2010	52	0
2011	72	4
2012	104	8
2013	86	3
2014	94	1
2015	127	7
Total	608	23

Figure 2 shows the number of CIR- and CME-driven geomagnetic storms per year and the total geomagnetic storms observed in the period 2008-2015. Most CIR-driven storms were observed during the declining phase of solar cycle 24 in

2015. This is because during the declining phase, the sunspot number (SSN) is normally lower than during solar maximum phase [45]. The largest CIR-driven geomagnetic storms were recorded in 2008, 2009, and 2010 with minimum Dst of −86, −83 and −81 respectively. The CME-driven geomagnetic storms, on the other hand, were dominant in 2012 which was one of the years with high solar activity in solar cycle 24. This result is in agreement with the previous studies [13] [46] that CIR- and CME-driven storms occur during the solar minimum/declining phase and solar maximum phase of the solar cycle, respectively. [47] studied the CME-driven storms (Dst ≤ −100 nT) during the rising and maximum phase of solar cycle 23 and found that the occurrence and intensity of the storms follow the known solar activity dependence, most frequent and more intense at solar maximum than at solar minimum. **Figure 3** illustrates the seasonal distribution of CIR- and CME-driven geomagnetic storms for the time period 2008-2015. Most CME-driven storms were observed during the March and September equinoxes, which is consistent with literature [13] [48]. The fact that more intense and numerous geomagnetic storms occur during the equinoxes than at the solstice has been reported [48] [49]. [48] attributed the seasonal variation of the geomagnetic activity with the polarity of interplanetary magnetic field, which emerges from the changing orientation of the solar equatorial coordinate system. During the equinoxes, the Earth's magnetic field is more likely to be disturbed by solar events because the direction of the axis of the Earth's magnetic field is more nearly at right angles to the flow of solar wind [50]. The CIR-driven storms were also mostly observed in the equinox months, which contradicts the previous studies that showed that CIR-driven storms occur mostly in the solstice seasons [13]. This could be attributed to the fact that interaction regions produced by high speed streams occur within the solar cycle and can drive nonrecurring geomagnetic activity [15]. The maximum geomagnetic activity which drives the formation of a storm occurs near the equinoxes and the minimum activity near the solstices [48]. Variation in geomagnetic activity has been attributed to the axial hypothesis, in which the heliographic latitude of the Earth plays a role, and the equinoctial hypothesis, in which the orientation of the Earth's axis of rotation relative to the Earth-Sun line plays a role [51].

To derive the relationship between magnetometer observations and C/NOFS satellite $\mathbf{E} \times \mathbf{B}$ drifts, direct comparison between magnetometer-derived ΔH was only considered at times when C/NOFS data were available. There were however few instances where C/NOFS data were available with no corresponding magnetometer data, and these cases were not included in the analysis. For example, in 2009, ΔH measurements were missing. **Figures 4-7** show local daytime changes in H component after removing the nighttime baseline value over Addis Ababa and Adigrat for the years 2008, 2010, 2011 and 2012, respectively. Superimposed on the ΔH (nT) plots are available C/NOFS satellite vertical ion plasma drift ($\mathbf{E} \times \mathbf{B}$ drift indicated as orange dots). These four years have been considered to obtain a clear relationship for which the magnetometer data was readily available. In **Figure 4**, there is an agreement between the C/NOFS $\mathbf{E} \times \mathbf{B}$ drift and ΔH

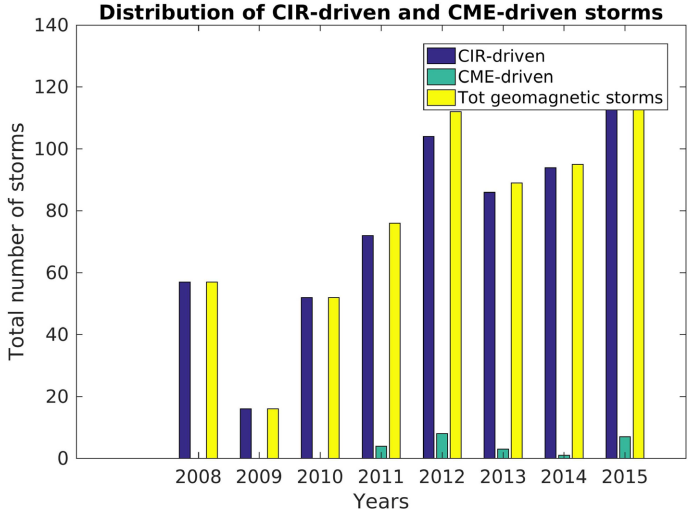

Figure 2. Distribution of CIR-, CME-driven storms and total number of geomagnetic storms from 2008-2015.

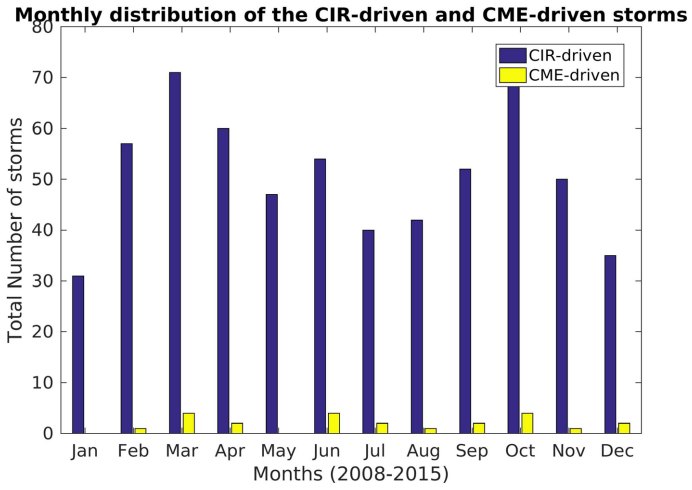

Figure 3. Monthly distribution of the CIR-driven storms (purple) and CME-driven storms (yellow) from 2008-2015.

in identifying upward vertical drifts and downward vertical drifts. However there is also a noticeable difference on 10 November 2008 where ΔH was mostly negative between 1300 LT and 1700 LT (corresponding to downward vertical drifts) while C/NOFS $\mathbf{E} \times \mathbf{B}$ drift observations show upward vertical drifts. In **Figure 5**, there is agreement in almost all periods between C/NOFS $\mathbf{E} \times \mathbf{B}$ drift observations and ΔH in identifying upward and downward vertical drifts. However, there is a visible difference on 04 April 2010 where C/NOFS observations were negative between 0700 LT and 0900 LT (corresponding to downward vertical drifts), while ΔH was positive (corresponding to upward vertical drifts). In **Figure 6** and **Figure 7**, there is an agreement in all the periods between ΔH data and C/NOFS $\mathbf{E} \times \mathbf{B}$ drift observations in identifying either upward or downward vertical drifts. [44] found out that there was a correlation value of 0.50 between C/NOFS vertical $\mathbf{E} \times \mathbf{B}$ drifts and ΔH for AAE for the year 2008. Although this correlation

seemed low, earlier studies had reported comparable results using satellite and magnetometer observations. For example, [52] showed that the correlation values over the Indian and Japanese sectors were ≈0.61 and 0.56 respectively using **E** × **B** drift obtained from ROCSAT-1 and EEJ (from ground-magnetometer data). The low correlation values were attributed to the altitude differences at which C/NOFS (or ROCSAT-1) vertical **E** × **B** drift and ΔH are computed. ΔH represents EEJ which is typically in the E region (about 110 km), while the C/NOFS vertical ion plasma drift (equivalent to vertical **E** × **B** drift at 400 km) was estimated within an altitude range of 400 - 550 km. Furthermore, the variation of neutral wind velocity with respect to altitude in low latitudes can alter the ground magnetic perturbation a few degrees off the magnetic equator [53] [54] and therefore contribute to the differences between derived ΔH and C/NOFS vertical **E** × **B** drift observations. From the four years considered (2008, 2010, 2011 and 2012), ΔH data and C/NOFS **E** × **B** drift data agreed in identifying either upward or downward vertical drifts.

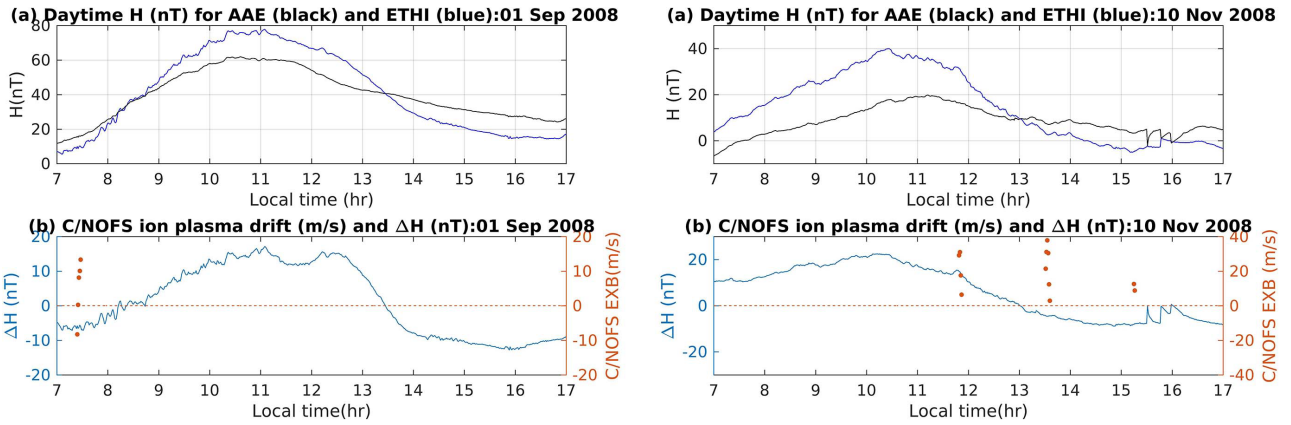

Figure 4. (a) Daytime H (nT) after removing the background H value over Addis Ababa (black curve) and Adigrat (blue) for 1 September 2008 on the left and 10 November 2008 on the right, (b) H (nT) obtained using data in (a), along with available C/NOFS vertical ion plasma drift (m/s) (**E** × **B** drift, plotted as orange dots) for 1 September 2008 on the left and 10 November 2008 on the right.

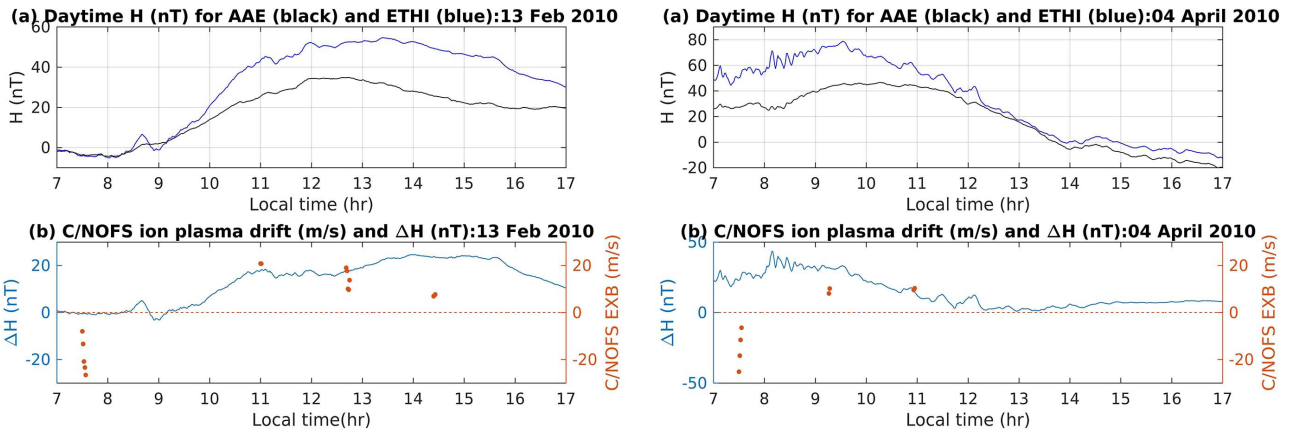

Figure 5. Comparison of H-component and C/NOFS vertical drifts for February 13, 2010 (left) and April 4, 2010 (right), similar to **Figure 4**.

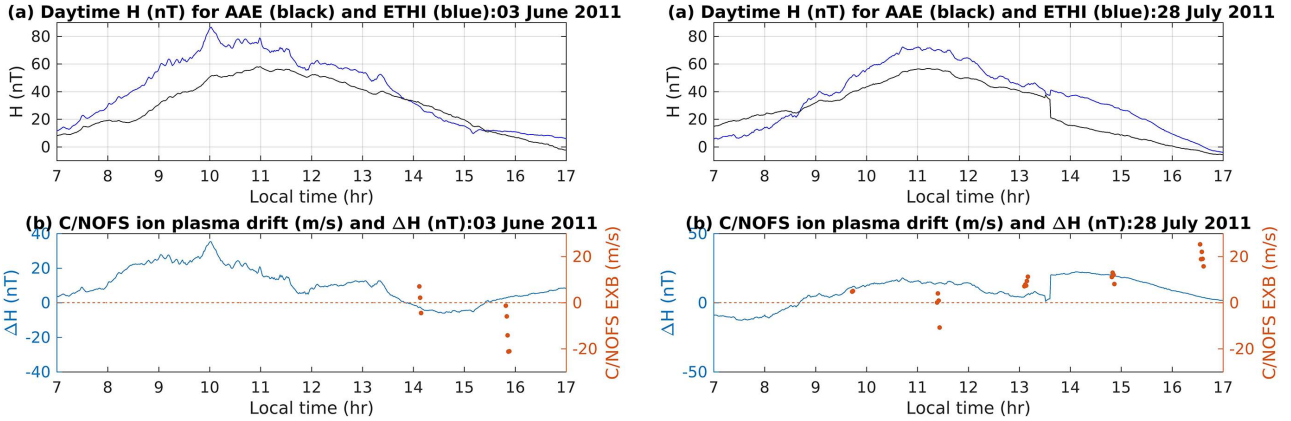

Figure 6. Comparison of *H*-component and C/NOFS vertical drifts for June 3, 2011 (left) and July 28, 2011 (right), similar to **Figure 4**.

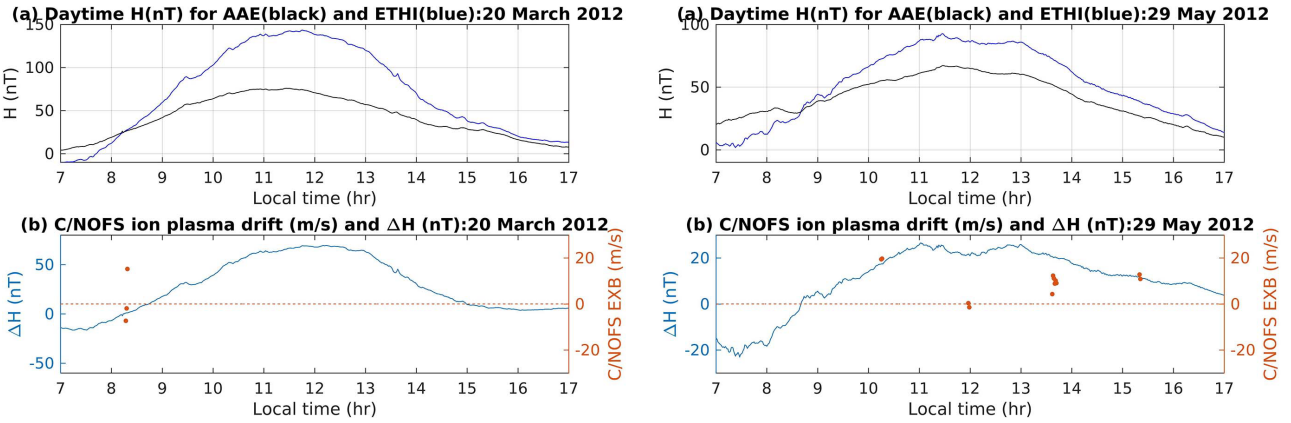

Figure 7. Comparison of *H*-component and C/NOFS vertical drifts for March 20, 2012 (left) and May 29, 2012 (right), similar to **Figure 4**.

To observe the geomagnetic storm effects on the ionospheric vertical drifts, we considered the effects due to CIR- and CME-driven storms separately. **Figure 8** shows the selected CIR-driven geomagnetic storms in the years 2010, 2011 and 2012 respectively. From **Figure 8** (top left panel), the storm started on 10 October 2010 with storm sudden commencement (SSC) occurrence at 1820 LT which led to the 11 October 2010 storm. The main phase of this storm started at 1800 LT on 11 October 2010 with the Dst reaching a value of −81 nT. During the main phase of this storm, $\mathbf{E} \times \mathbf{B}$ drift decreased due to reduction in ΔH after the SSC which is manifested as downward $\mathbf{E} \times \mathbf{B}$ drifts. This is a result of disturbance dynamo electric field contribution at low latitudes during daytime [33]. The $\mathbf{E} \times \mathbf{B}$ drift variations implied, the electric field changes at equatorial station, which also altered the equatorial $\mathbf{E} \times \mathbf{B}$ drifts [21]. The storm of 03-07 February 2011 (**Figure 8** top right panel) started with a SSC at 1400 LT on 04 February 2011 and its main phase continued into the next day with Dst value reaching −60 nT on 05 February 2011. The $\mathbf{E} \times \mathbf{B}$ drift decreased during the main phase of this storm, which is a manifestation of downward $\mathbf{E} \times \mathbf{B}$ associated with westward electric field. The penetration electric fields are usually westward in the midnight to dawn sector [55]

and this explains the strong downward **E** × **B** associated with the observations on 05 February 2011. The storm of 07-11 July 2012 storm (shown in Figure 8 bottom left panel) started with a SSC at 1900 LT 0n 08 July 2012. There was a temporary sudden increase in **E** × **B** drift during the SSC. The main phase of this storm occurred on 09 July 2012 with the Dst reaching a value of -86 nT. There was also a decrease in **E** × **B** drift during the main phase of this storm. This is a manifestation of down-ward **E** × **B** drifts associated with westward electric field which could be due to the disturbance dynamo contribution. Electric fields of ionospheric disturbance dynamo origin can reverse the low-latitude daytime eastward electric field [33]. It is also evident that **E** × **B** drift was negative for most hours on 09 July 2012. This indicates that the equatorial electric fields remained suppressed during most times of storm event. This could be attributed to the longer period taken during the recovery phase [23].

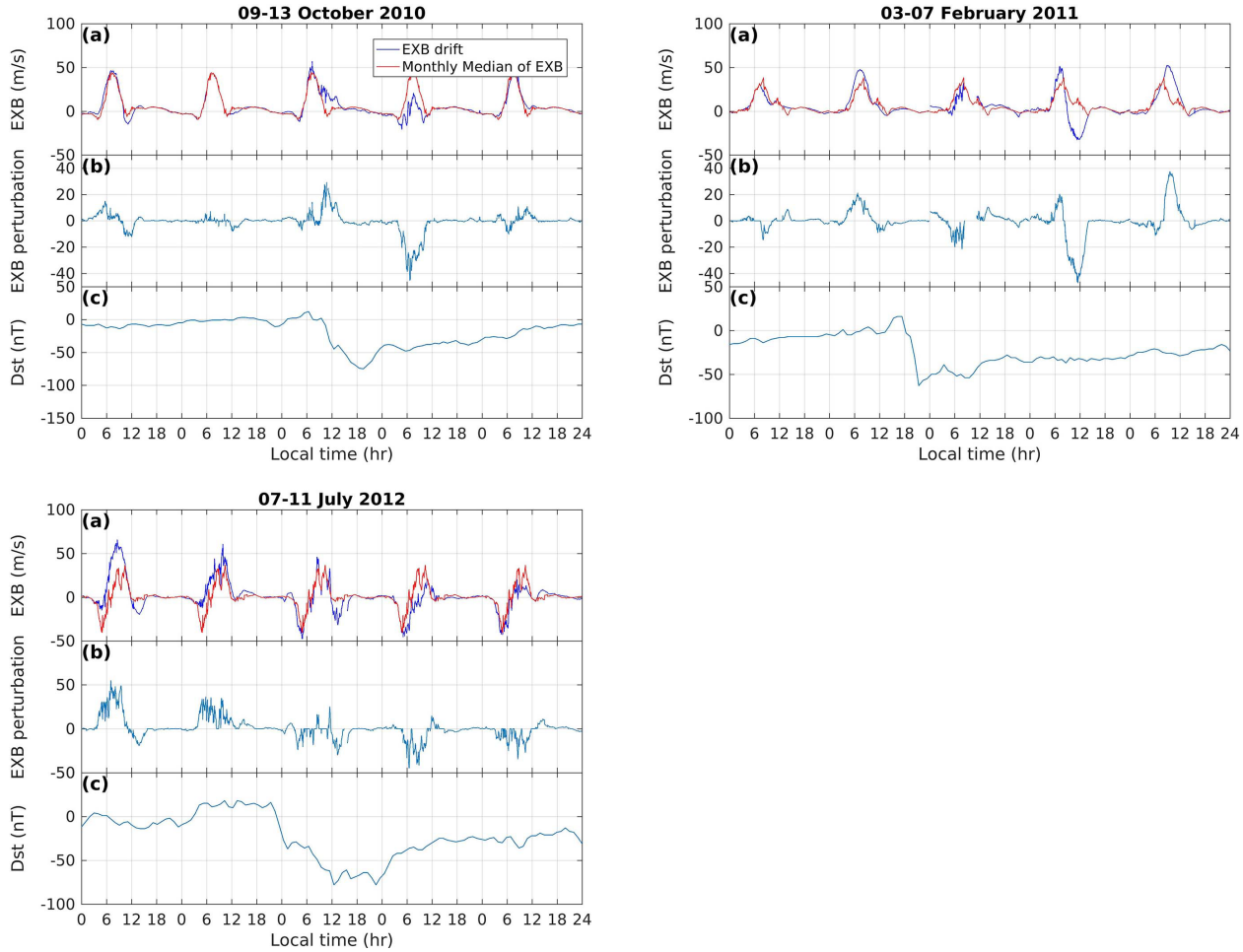

Figure 8. CIR-driven geomagnetic storms; Panels from top to bottom show the variations of (a) **E** × **B** of a day and corresponding monthly median (nT); (b) **E** × **B** perturbation; (c) Dst (nT) as a function of Local time, two days before and after the storm day for 09-13 October 2010 storm on the left and 03-07 February 2011 storm on the right, and 07-11 July 2012 on the bottom left panel.

Figure 9 shows CME-driven geomagnetic storms of the year 2012. The analysis was made for the year 2012 because it was the year in which most CME-driven

storms were observed and there was corresponding magnetometer $\mathbf{E} \times \mathbf{B}$ drift data for the observed storms. The 0711 March 2012 storm started with a sudden storm commencement (SSC) occurrence at 0420 LT. This was followed by another SSC on 8 March 2012 at 1100 LT, which led to the 9 March storm. Although the SSC occurred on 8 March at 1100 LT, the main phase started more than about 12 hours later at 0100 LT on 9 March 2012, with the Dst reaching a value of −145 nT (at 0800 LT). The shock of 8 March 2012 at 1100 LT led to a temporary sudden increase in $\mathbf{E} \times \mathbf{B}$ drift due to an increase in ΔH, while the rest of the daytime decrease in ΔH is a manifestation of downward $\mathbf{E} \times \mathbf{B}$ drifts associated with westward electric field. This could be due to the disturbance dynamo contribution that lasted long after the 7 March storm. Electric fields of ionospheric disturbance dynamo origin can reverse the low-latitude daytime eastward electric field [33] [56], and it has been shown both numerically [2] and with observations [57] that the imposed westward electric field has the potential to be present for long hours (in the order of hours to a day) even after the maximum geomagnetic activity has returned to normal. On 9 March 2012, there was an enhancement of the eastward electric field leading to an increase in $\mathbf{E} \times \mathbf{B}$ drift from about 0600 LT to 0900 LT. The 13-17 July 2012 storm started with a SSC at 1810 LT on 14 July 2012 and its main phase continued into the next day with Dst reaching a value of −139 nT on 15 July. Although there is no ΔH on 15 July 2012, it has been shown (using a single equatorial station) that $\mathbf{E} \times \mathbf{B}$ drifts from magnetometer data increased between 0900 - 1100 LT [24]. [56] found out that, there was an increase in $\mathbf{E} \times \mathbf{B}$ drifts due to an increase in ΔH and increase in interplanetary electric fields during this time interval, and suggested that this could have led to penetration of electric fields of magnetospheric origin to low latitudes, which are eastward during daytime. The eastward electric field enhances equatorial latitude vertical $\mathbf{E} \times \mathbf{B}$ drifts.

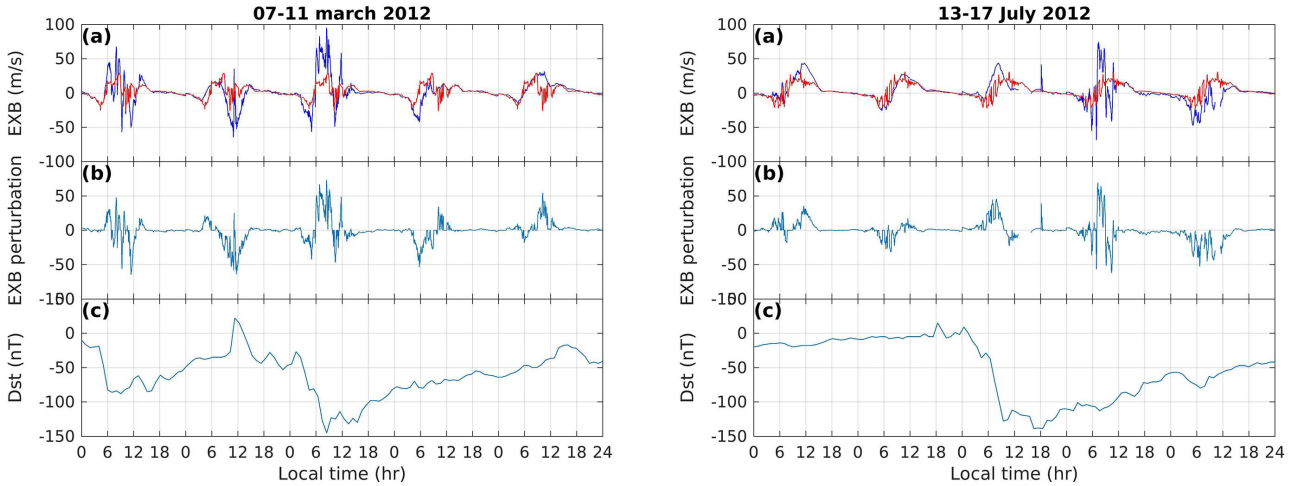

Figure 9. Similar to **Figure 8** but for CME-driven geomagnetic storms of 07-11 March 2012, and 13-17 July 2012.

4. Conclusions and Suggestions

This study focused on analysis of the geomagnetic storm effects on ionospheric

vertical drifts over the East African low latitude region using magnetometer data, C/NOFS data, Dst and Kp indices. A total of 608 CIR-driven and 23 CME-driven geomagnetic storms were identified for the period 2008-2015. Most CIR-driven storms were observed during the declining phase of solar cycle 24 in 2015. The CME-driven geomagnetic storms, on the other hand, were dominant during one of the near maximum phase of the solar cycle 24 (*i.e.*, in 2012). The CIR-driven storms were mostly observed in the March and September equinoxes, which contradicts the previous studies that showed that CIR-driven storms occur mostly in the solstice seasons. This could be attributed to the fact that interaction regions (IRs) produced by high-speed streams occur within the solar cycle and can drive nonrecurring geomagnetic activity. There was agreement in almost all periods between C/NOFS $\mathbf{E} \times \mathbf{B}$ drifts data and ΔH in identifying either upward or downward vertical drifts. It was found that an enhancement in $\mathbf{E} \times \mathbf{B}$ drifts during both CIR- and CME-driven geomagnetic storms was due to the presence of PPEFs. We also observed downward $\mathbf{E} \times \mathbf{B}$ drifts during CIR-driven geomagnetic storms, which are associated with westward electric field due to disturbance dynamo. This study confirms that the ionospheric plasma dynamics in the East African low latitude region are primarily governed by the east-west electric field, influencing vertical drifts significantly. Findings from this study can be used to assess whether similar mechanisms dominate in other non-African low-latitude regions, enhancing the global picture of ionospheric storm responses. Statistical analysis should be carried out over longer time periods using other satellite missions like Swarm satellite to determine which storm categories mostly influence ionospheric vertical drifts, and this forms a basis for modelling the response of ionospheric vertical drifts to geomagnetic storms. Furthermore, extraction of Ddyn and DP2 currents should be done to rule out the separate contributions of DDEF and PPEF to ionospheric vertical drifts during geomagnetic storms.

Acknowledgements

The authors acknowledge financial support from the Swedish International Development Agency (SIDA) through the International Science Programme (ISP) of Uppsala University in Sweden. The Dst and kp indices were downloaded from Kyoto website: https://omniweb.gsfc.nasa.gov/form/dx1.html. The C/NOFS satellite data was downloaded from http://spdf.gsfc.nasa.gov/pub/data/cnofs/cindi/.

Author Contributions

VH prepared the manuscript. DN, VH and EJ designed and conducted the current research. DN carried out the analysis of the data. VH interpreted the results, and edited the draft manuscript together with DN and EJ. All authors read and approved the final manuscript.

Availability of Data and Materials

All data is publicly available on their corresponding websites.

Conflicts of Interest

The authors declare that they have no competing interests.

References

[1] Sobral, J.H.A., Abdu, M.A., Yamashita, C.S., Gonzalez, W.D., de Gonzalez, A.C., Batista, I.S., *et al.* (2001) Responses of the Low-Latitude Ionosphere to Very Intense Geomagnetic Storms. *Journal of Atmospheric and Solar-Terrestrial Physics*, **63**, 965-974. https://doi.org/10.1016/s1364-6826(00)00197-8

[2] Huang, C., Foster, J.C. and Kelley, M.C. (2005) Long-Duration Penetration of the Interplanetary Electric Field to the Low-Latitude Ionosphere during the Main Phase of Magnetic Storms. *Journal of Geophysical Research*: *Space Physics*, **110**, A11309. https://doi.org/10.1029/2005ja011202

[3] Uga, C.I., Gautam, S.P. and Seba, E.B. (2024) TEC Disturbances Caused by CME-Triggered Geomagnetic Storm of September 6-9, 2017. *Heliyon*, **10**, e30725. https://doi.org/10.1016/j.heliyon.2024.e30725

[4] Nava, B., Rodríguez-Zuluaga, J., Alazo-Cuartas, K., Kashcheyev, A., Migoya-Orué, Y., Radicella, S.M., *et al.* (2016) Middle- and Low-Latitude Ionosphere Response to 2015 St. Patrick's Day Geomagnetic Storm. *Journal of Geophysical Research*: *Space Physics*, **121**, 3421-3438. https://doi.org/10.1002/2015ja022299

[5] Mansilla, G.A. (2006) Equatorial and Low Latitude Ionosphere during Intense Geomagnetic Storms. *Journal of Atmospheric and Solar-Terrestrial Physics*, **68**, 2091-2100. https://doi.org/10.1016/j.jastp.2006.07.005

[6] Klimenko, M.V., Klimenko, V.V., Ratovsky, K.G., Goncharenko, L.P., Sahai, Y., Fagundes, P.R., *et al.* (2011) Numerical Modeling of Ionospheric Effects in the Middle- and Low-Latitude *F* Region during Geomagnetic Storm Sequence of 9-14 September 2005. *Radio Science*, **46**, RS0D03. https://doi.org/10.1029/2010rs004590

[7] Ratovsky, K.G., Klimenko, M.V., Yasyukevich, Y.V., Klimenko, V.V. and Vesnin, A.M. (2020) Statistical Analysis and Interpretation of High-, Mid- and Low-Latitude Responses in Regional Electron Content to Geomagnetic Storms. *Atmosphere*, **11**, Article 1308. https://doi.org/10.3390/atmos11121308

[8] Adhikari, B., Klausner, V., Cândido, C.M.N., Poudel, P., Gimenes, H.M., Silwal, A., *et al.* (2024) Lithosphere-Atmosphere-Ionosphere Coupling during the September 2015 Coquimbo Earthquake. *Journal of Earth System Science*, **133**, Article No. 35. https://doi.org/10.1007/s12040-023-02222-x

[9] Olatunbosun, L.G. (2022) Prompt Penetration Electric Field and the Ionospheric Effects of Major Geomagnetic Storms in Low Latitude Stations. *International Research Journal of Innovations in Engineering and Technology*, **6**, 61-67.

[10] Abdu, M.A. (2012) Equatorial Spread F/Plasma Bubble Irregularities under Storm Time Disturbance Electric Fields. *Journal of Atmospheric and Solar-Terrestrial Physics*, **75**, 44-56. https://doi.org/10.1016/j.jastp.2011.04.024

[11] Gonzalez, W.D., Joselyn, J.A., Kamide, Y., Kroehl, H.W., Rostoker, G., Tsurutani, B.T., *et al.* (1994) What Is a Geomagnetic Storm? *Journal of Geophysical Research*: *Space Physics*, **99**, 5771-5792. https://doi.org/10.1029/93ja02867

[12] Kamide, Y., Yokoyama, N., Gonzalez, W., Tsurutani, B.T., Daglis, I.A., Brekke, A., *et al.* (1998) Two-Step Development of Geomagnetic Storms. *Journal of Geophysical Research*: *Space Physics*, **103**, 6917-6921. https://doi.org/10.1029/97ja03337

[13] Matamba, T.M. and Habarulema, J.B. (2018) Ionospheric Responses to CME- and CIR-Driven Geomagnetic Storms along 30˚E-40˚E over the African Sector from 2001

to 2015. *Space Weather*, **16**, 538-556. https://doi.org/10.1029/2017sw001754

[14] Moldwin, M. (2022) An Introduction to Space Weather. 2nd Edition, Cambridge University Press. https://doi.org/10.1017/9781108866538

[15] Borovsky, J.E. and Denton, M.H. (2006) Differences between CME-Driven Storms and CIR-Driven Storms. *Journal of Geophysical Research*: *Space Physics*, **111**, A07S08. https://doi.org/10.1029/2005ja011447

[16] Tsurutani, B.T., Gonzalez, W.D., Gonzalez, A.L.C., Guarnieri, F. L., *et al.* (2006) Corotating Solar Wind Streams and Recurrent Geomagnetic Activity: A Review. *Journal of Geophysical Research*: *Space Physics*, **111**, A07S01.

[17] Qiu, N., Chen, Y.H., Wang, W.B., Gong, J.C. and Liu, S.Q. (2015) Statistical Analysis of the Ionosphere Response to the CIR and CME in Mid-Latitude Regions. *Chinese Journal of Geophysics*, **58**, 2250-2262.

[18] Calabia, A., Anoruo, C., Shah, M., Amory-Mazaudier, C., Yasyukevich, Y., Owolabi, C., *et al.* (2022) Low-Latitude Ionospheric Responses and Coupling to the February 2014 Multiphase Geomagnetic Storm from GNSS, Magnetometers, and Space Weather Data. *Atmosphere*, **13**, Article 518. https://doi.org/10.3390/atmos13040518

[19] Gautam, S.P., Adhikari, L., Zank, G.P., Silwal, A. and Zhao, L. (2024) Solar Cycle Dependence of the Turbulence Cascade Rate at 1 Au. *The Astrophysical Journal*, **968**, Article 12. https://doi.org/10.3847/1538-4357/ad4797

[20] Yizengaw, E., Moldwin, M.B., Mebrahtu, A., Damtie, B., Zesta, E., Valladares, C.E., *et al.* (2011) Comparison of Storm Time Equatorial Ionospheric Electrodynamics in the African and American Sectors. *Journal of Atmospheric and Solar-Terrestrial Physics*, **73**, 156-163. https://doi.org/10.1016/j.jastp.2010.08.008

[21] Veenadhari, B., Kumar, S., Tulasi Ram, Singh, R. and Alex, S. (2012) Corotating Interaction Region (CIR) Induced Magnetic Storms during Solar Minimum and Their Effects on Low-Latitude Geomagnetic Field and Ionosphere. *Indian Journal of Radio and Space Physics*, **41**, 306-315.

[22] Buresova, D., Lastovicka, J., Hejda, P. and Bochnicek, J. (2014) Ionospheric Disturbances under Low Solar Activity Conditions. *Advances in Space Research*, **54**, 185-196. https://doi.org/10.1016/j.asr.2014.04.007

[23] Joseph, O.O., Yamazak, Y., Cilliers, P., Baki, P., Ngwira, C.M. and Mito, C. (2015) A Study on the Response of the Equatorial Ionization Anomaly over the East Africa Sector during the Geomagnetic Storm of November 13, 2012. *Advances in Space Research*, **55**, 2863-2872. https://doi.org/10.1016/j.asr.2015.03.011

[24] Tesema, F., Damtie, B. and Nigussie, M. (2015) The Response of the Ionosphere to Intense Geomagnetic Storms in 2012 Using GPS-TEC Data from East Africa Longitudinal Sector. *Journal of Atmospheric and Solar-Terrestrial Physics*, **135**, 143-151. https://doi.org/10.1016/j.jastp.2015.10.021

[25] Matamba, T.M., Habarulema, J.B. and McKinnell, L. (2015) Statistical Analysis of the Ionospheric Response during Geomagnetic Storm Conditions over South Africa Using Ionosonde and GPS Data. *Space Weather*, **13**, 536-547. https://doi.org/10.1002/2015sw001218

[26] Dugassa, T., Habarulema, J.B. and Nigussie, M. (2020) Statistical Study of Geomagnetic Storm Effects on the Occurrence of Ionospheric Irregularities over Equatorial/Low-Latitude Region of Africa from 2001 to 2017. *Journal of Atmospheric and Solar-Terrestrial Physics*, **199**, Article ID: 105198. https://doi.org/10.1016/j.jastp.2020.105198

[27] Veenadhari, B., Alex, S., Kikuchi, T., Shinbori, A., Singh, R. and Chandrasekhar, E.

(2010) Penetration of Magnetospheric Electric Fields to the Equator and Their Effects on the Low-Latitude Ionosphere during Intense Geomagnetic Storms. *Journal of Geophysical Research: Space Physics*, **115**, A03305. https://doi.org/10.1029/2009ja014562

[28] Kikuchi, T., Lühr, H., Schlegel, K., Tachihara, H., Shinohara, M. and Kitamura, T. (2000) Penetration of Auroral Electric Fields to the Equator during a Substorm. *Journal of Geophysical Research*: *Space Physics*, **105**, 23251-23261. https://doi.org/10.1029/2000ja900016

[29] Habyarimana, V., Habarulema, J.B., Mungufeni, P. and Uwamahoro, J.C. (2020) An Effort to Study the Influence of Tides on the Longitudinal Variation of Vertical E × B Drift over the African Sector. *Journal of Atmospheric and Solar-Terrestrial Physics*, **206**, Article ID: 105338. https://doi.org/10.1016/j.jastp.2020.105338

[30] Anderson, D., Anghel, A., Yumoto, K., Ishitsuka, M. and Kudeki, E. (2002) Estimating Daytime Vertical E × B Drift Velocities in the Equatorial F-Region Using Ground-based Magnetometer Observations. *Geophysical Research Letters*, **29**, 37-1-37-4. https://doi.org/10.1029/2001gl014562

[31] Fejer, B.G., Scherliess, L. and de Paula, E.R. (1999) Effects of the Vertical Plasma Drift Velocity on the Generation and Evolution of Equatorial Spread *F*. *Journal of Geophysical Research*: *Space Physics*, **104**, 19859-19869. https://doi.org/10.1029/1999ja900271

[32] Kil, H., Oh, S., Paxton, L.J. and Fang, T. (2009) High-Resolution Vertical E × B Drift Model Derived from ROCSAT-1 Data. *Journal of Geophysical Research*: *Space Physics*, **114**, A10314. https://doi.org/10.1029/2009ja014324

[33] Blanc, M. and Richmond, A.D. (1980) The Ionospheric Disturbance Dynamo. *Journal of Geophysical Research*: *Space Physics*, **85**, 1669-1686. https://doi.org/10.1029/ja085ia04p01669

[34] Fejer, B.G. (1997) The Electrodynamics of the Low-Latitude Ionosphere: Recent Results and Future Challenges. *Journal of Atmospheric and Solar-Terrestrial Physics*, **59**, 1465-1482. https://doi.org/10.1016/s1364-6826(96)00149-6

[35] Tilahun, S. (2021) Estimating the Daytime Vertical E × B Drift from Magnetometer and C/NOFS Measurements and Comparison with Empirical Models over the East African Sector. *Radio Science*, **56**, e2019RS007037. https://doi.org/10.1029/2019rs007037

[36] Anderson, D., Anghel, A., Chau, J. and Veliz, O. (2004) Daytime Vertical E × B Drift Velocities Inferred from Ground-Based Magnetometer Observations at Low Latitudes. *Space Weather*, **2**, S11001. https://doi.org/10.1029/2004sw000095

[37] Yizengaw, E., Moldwin, M.B., Zesta, E., Biouele, C.M., Damtie, B., Mebrahtu, A., *et al.* (2014) The Longitudinal Variability of Equatorial Electrojet and Vertical Drift Velocity in the African and American Sectors. *Annales Geophysicae*, **32**, 231-238. https://doi.org/10.5194/angeo-32-231-2014

[38] Rodrigues, F.S., Crowley, G., Azeem, S.M.I. and Heelis, R.A. (2011) C/NOFS Observations of the Equatorial Ionospheric Electric Field Response to the 2009 Major Sudden Stratospheric Warming Event. *Journal of Geophysical Research*: *Space Physics*, **116**, A09316. https://doi.org/10.1029/2011ja016660

[39] Stoneback, R.A., Davidson, R.L. and Heelis, R.A. (2012) Ion Drift Meter Calibration and Photoemission Correction for the C/NOFS Satellite. *Journal of Geophysical Research*: *Space Physics*, **117**, A08323. https://doi.org/10.1029/2012ja017636

[40] Rodrigues, F.S., Smith, J.M., Milla, M. and Stoneback, R.A. (2015) Daytime Ionospheric Equatorial Vertical Drifts during the 2008-2009 Extreme Solar Minimum.

Journal of Geophysical Research: *Space Physics*, **120**, 1452-1459. https://doi.org/10.1002/2014ja020478

[41] Stoneback, R.A., Heelis, R.A., Burrell, A.G., Coley, W.R., Fejer, B.G. and Pacheco, E. (2011) Observations of Quiet Time Vertical Ion Drift in the Equatorial Ionosphere during the Solar Minimum Period of 2009. *Journal of Geophysical Research*: *Space Physics*, **116**, A12327. https://doi.org/10.1029/2011ja016712

[42] Huber, P.J. and Ronchetti, E.M. (2011) Robust Statistics. John Wiley & Sons.

[43] Dubazane, M.B., Habarulema, J.B. and Uwamahoro, J.C. (2018) Modelling Ionospheric Vertical Drifts over Africa Low Latitudes Using Empirical Orthogonal Functions and Comparison with Climatological Model. *Advances in Space Research*, **61**, 326-336. https://doi.org/10.1016/j.asr.2017.10.024

[44] Habarulema, J.B., Lefebvre, G., Moldwin, M.B., Katamzi-Joseph, Z.T. and Yizengaw, E. (2019) Counter-Electrojet Occurrence as Observed from C/NOFS Satellite and Ground-Based Magnetometer Data over the African and American Sectors. *Space Weather*, **17**, 1090-1104. https://doi.org/10.1029/2019sw002236

[45] Wu, C., Liou, K., Lepping, R.P., Hutting, L., Plunkett, S., Howard, R.A., *et al.* (2016) The First Super Geomagnetic Storm of Solar Cycle 24: "The St. Patrick's Day Event (17 March 2015)". *Earth, Planets and Space*, **68**, Article No. 151. https://doi.org/10.1186/s40623-016-0525-y

[46] Tsurutani, B.T., McPherron, R.L., Gonzalez, W.D., Lu, G., Gopalswamy, N. and Guarnieri, F.L. (2006) Magnetic Storms Caused by Corotating Solar Wind Streams. In: Tsurutani, B., *et al.*, Eds., *Recurrent Magnetic Storms: Corotating Solar Wind Streams*, American Geophysical Union, 1-17. https://doi.org/10.1029/167gm03

[47] Vijaya Lekshmi, D., Balan, N., Tulasi Ram, S. and Liu, J.Y. (2011) Statistics of Geomagnetic Storms and Ionospheric Storms at Low and Mid Latitudes in Two Solar Cycles. *Journal of Geophysical Research*: *Space Physics*, **116**, A11328. https://doi.org/10.1029/2011ja017042

[48] Russell, C.T. and McPherron, R.L. (1973) Semiannual Variation of Geomagnetic Activity. *Journal of Geophysical Research*, **78**, 92-108. https://doi.org/10.1029/ja078i001p00092

[49] Mursula, K., Tanskanen, E. and Love, J.J. (2011) Spring-Fall Asymmetry of Substorm Strength, Geomagnetic Activity and Solar Wind: Implications for Semiannual Variation and Solar Hemispheric Asymmetry. *Geophysical Research Letters*, **38**, L06104. https://doi.org/10.1029/2011gl046751

[50] Häkkinen, L.V.T., Pulkkinen, T.I., Pirjola, R.J., Nevanlinna, H., Tanskanen, E.I. and Turner, N.E. (2003) Seasonal and Diurnal Variation of Geomagnetic Activity: Revised *Dst* versus External Drivers. *Journal of Geophysical Research*: *Space Physics*, **108**, 1060. https://doi.org/10.1029/2002ja009428

[51] Cortie, A.L. (1912) Sun-Spots and Terrestrial Magnetic Phenomena, 1898-1911: The Cause of the Annual Variation in Magnetic Disturbances. *Monthly Notices of the Royal Astronomical Society*, **73**, 52-60. https://doi.org/10.1093/mnras/73.1.52

[52] Kumar, S., Veenadhari, B., Tulasi Ram, S., Su, S. and Kikuchi, T. (2016) Possible Relationship between the Equatorial Electrojet (EEJ) and Daytime Vertical E × B Drift Velocities in F Region from ROCSAT Observations. *Advances in Space Research*, **58**, 1168-1176. https://doi.org/10.1016/j.asr.2016.06.009

[53] Fambitakoye, O., Mayaud, P.N. and Richmond, A.D. (1976) Equatorial Electrojet and Regular Daily Variation SR—III. Comparison of Observations with a Physical Model. *Journal of Atmospheric and Terrestrial Physics*, **38**, 113-121. https://doi.org/10.1016/0021-9169(76)90118-5

[54] Fang, T.W., Richmond, A.D., Liu, J.Y. and Maute, A. (2008) Wind Dynamo Effects on Ground Magnetic Perturbations and Vertical Drifts. *Journal of Geophysical Research*: *Space Physics*, **113**, A11313. https://doi.org/10.1029/2008ja013513

[55] Fejer, B.G. (1991) Low Latitude Electrodynamic Plasma Drifts: A Review. *Journal of Atmospheric and Terrestrial Physics*, **53**, 677-693. https://doi.org/10.1016/0021-9169(91)90121-m

[56] Habarulema, J.B., Katamzi, Z.T., Sibanda, P. and Matamba, T.M. (2017) Assessing Ionospheric Response during Some Strong Storms in Solar Cycle 24 Using Various Data Sources. *Journal of Geophysical Research*: *Space Physics*, **122**, 1064-1082. https://doi.org/10.1002/2016ja023066

[57] Yamazaki, Y. and Kosch, M.J. (2015) The Equatorial Electrojet during Geomagnetic Storms and Substorms. *Journal of Geophysical Research*: *Space Physics*, **120**, 2276-2287. https://doi.org/10.1002/2014ja020773

List of Abbreviations

GNSS:	Global Navigation Satellite System
IMF Bz:	z-component of the Interplanetary magnetic field
HSSWS:	High speed solar wind stream
CME:	Coronal mass ejection
CIR:	Corotating interaction region
PPEF:	Prompt penetration electric field
IGS:	International GNSS Service
DDEF:	Disturbance dynamo electric field
C/NOFS:	Communication/Navigation Outage and Forecasting System
PRE:	Pre-reversal enhancement